Journal of The Electrochemical Society, **156** (4) A289-A293 (2009)
0013-4651/2009/156(4)/A289/5/$23.00 © The Electrochemical Society

Capacity-Fading Mechanisms of $LiNiO_2$-Based Lithium-Ion Batteries

I. Analysis by Electrochemical and Spectroscopic Examination

Tsuyoshi Sasaki,[a,*,z] Takamasa Nonaka,[a] Hideaki Oka,[a] Chikaaki Okuda,[a] Yuichi Itou,[a] Yasuhito Kondo,[a] Yoji Takeuchi,[a] Yoshio Ukyo,[a,*] Kazuyoshi Tatsumi,[b] and Shunsuke Muto[b,*]

[a]*Toyota Central Research and Development Laboratories, Incorporated, Nagoakute 480-1192, Japan*
[b]*Department of Materials, Physics and Energy Engineering, Graduate School of Engineering, Nagoya University, Chikusa-ku, Nagoya 464-8603, Japan*

The mechanism for capacity fade of lithium-ion batteries with $LiNi_{0.8}Co_{0.15}Al_{0.05}O_2$ as a positive electrode material associated with cycling at elevated temperatures was investigated by the combination of electrochemical and spectroscopic methods. The total capacity fade of the battery after charge/discharge cycle test at 80°C was found to be almost explained by the capacity fade of the positive electrode, which indicates that the degradation of the positive electrode is mainly responsible for capacity fade of the battery at this temperature. Quantitative analyses revealed a strong positive correlation between the capacity fade of the positive electrode and the amount of inactive Ni ions in the active material after the cycling test. It is concluded that the capacity fade is mainly caused by the formation of inactive Ni(II) and Ni(III), presumably associated with oxygen loss in the active materials, which act as obstacles to Li intercalation/deintercalation.
 [DOI: 10.1149/1.3076136]

Manuscript submitted October 29, 2008; revised manuscript received December 19, 2008. Published February 4, 2009.

Lithium-ion batteries have drawn significant attention as power sources due to their high energy density and excellent power performance. $LiNiO_2$-based positive electrode materials have been considered as one of the most promising candidates to replace lithium cobalt oxide ($LiCoO_2$) because of their good electrochemical performance.[1,2] Among them, Co and Al codoped $LiNiO_2$-based materials have attracted attention due to their relatively good thermal stability and cyclability.[3-6]

However, lithium-ion batteries using $LiNiO_2$-based materials still suffer from deterioration of properties such as capacity fade and increase in impedance by cycling or aging at elevated temperatures.[7-13] Some researchers have reported that the interfacial resistance at the positive electrode is the main reason behind the increased impedance of the battery.[14-16] We have also confirmed that the increase in resistance of the battery after cycling at 60°C was mainly attributed to the increase in positive electrode resistance.[10]

Many studies on positive electrodes have been conducted to elucidate the structural changes that result from cycling or aging. Several changes were reported for degraded positive electrodes: (*i*) formation of NiO-like surface layers in active materials,[17,18] (*ii*) formation of cracks in active materials,[10] (*iii*) formation of a solid electrolyte interphase (SEI) layer on active materials,[9,19,20] (*iv*) loss of carbon from the surfaces of positive electrodes,[9] (*v*) corrosion of aluminum current collectors,[21] and (*vi*) increase in electronic contact resistance between electrode components within positive electrodes.[20,22]

However, the quantitative relationship between the deterioration of electrochemical properties and structural/chemical changes of positive electrodes is still unclear. Therefore, the factors that mainly affect the battery performance should be determined, specifically whether or not the degradation in battery performance is actually attributable to degradation of the active material itself. We have previously reported the presence of lower valence Ni in positive electrodes after cycling or aging at 60°C compared with that of noncycled/aged electrode.[23] However, according to Kobayashi et al.,[24] the bulk structure of the positive electrode essentially remained unchanged, even after battery degradation at elevated temperatures. This discrepancy is presumed to depend on the extent that the damages proceed, and therefore quantitative analyses are necessary.

* Electrochemical Society Active Member.
z E-mail: sasakit@mosk.tytlabs.co.jp

In the present study, we focus on the capacity-fade mechanism of positive electrodes after cycling tests at 20–80°C, because capacity fade is a more-essential issue of battery degradation than increase of resistance. The purpose of this first part in a series of papers is (*i*) to settle the controversy as to where positive electrode degradation takes place and (*ii*) to deduce a quantitative relation between capacity fade and the structural degradation of the positive electrode material utilizing not only electrochemical techniques but also spectroscopic techniques. Clarification of the regions in the positive electrode that are actually damaged, and the extent of the damage, will provide essential guiding principles for the development of $LiNiO_2$-based positive electrodes.

Experimental

Cylindrical cell preparation.— Charge–discharge cycling tests were carried out using 500 mAh type cylindrical cells. The cell consisted of a positive electrode, a negative electrode, a 1 M $LiPF_6$ electrolyte dissolved in a solvent of 3:7 (by volume) ethylene carbonate/diethyl carbonate (EC/DEC), and a microporous polyethylene separator. Fabrication details of the cylindrical cell used in this study are described elsewhere.[10] The positive electrode sheet was a thin Al current collector coated on both sides with 20 μm thick electrode mixtures, composed of 85 wt % $LiNi_{0.8}Co_{0.15}Al_{0.05}O_2$, 10 wt % conductive material, and 5 wt % polyvinylidene fluoride (PVdF) binder. $LiNi_{0.8}Co_{0.15}Al_{0.05}O_2$ was prepared by a coprecipitation method.[13] The anode sheet was a thin Cu foil coated with 95 wt % artificial graphite and 5 wt % PVdF binder.

Cycling test.— In the present study, cells were prepared that exhibited various levels of capacity fade: fresh cells and cells cycle-tested for 500 cycles at 20, 60, 70, and 80°C. Cycling tests were carried out at 2.0 mA cm^{-1} (~2 C rate) in the range from 3.0 to 4.1 V.

To determine the reversible capacity, the cells were charged under constant voltage to 4.1 V before and after cycling tests and discharged at 0.2 mA cm^{-1} (~0.1 C rate) to 3.0 V at 20°C.

The batteries were disassembled in an argon-filled glove box before and after cycling tests for extraction of the positive electrodes. After disassembling, the positive electrodes were washed in DEC. Three electrode half-cells were fabricated to measure the electrochemical properties of the positive electrodes. Li metal was used as a counter electrode and a reference electrode, and 1 M $LiPF_6$ dissolved in an EC/DEC solvent (3:7 in volume) was applied as an electrolyte solution. To determine the capacity fade of the positive

electrodes the three electrode half-cells were charged to 4.2 V and discharged to 3.0 V at 20°C using constant current–constant voltage (CC-CV) protocol. Charging and discharging were performed at 0.2 mA cm^{-1} (~0.1 C rate) during the constant current part. Subsequently, the voltage was kept constant for 2 h. In addition, cyclic voltammetry was conducted using an electrochemical analyzer (HZ-5000, Hokuto Denko) in the potential range between 3.0 and 4.5 V at a scan rate of 0.2 mV s^{-1} and at 20°C.

XRD and SEM measurements.— X-ray diffraction (XRD) measurements were carried out on each positive electrode before and after cycling tests at 60 and 80°C using RINT-2200 (Rigaku Corp.) with Cu Kα radiation. To examine corrosion of the Al current collector, the cross sections of the electrodes before and after cycling test at 80°C were observed by scanning electron microscope (SEM, S-4300, Hitachi). However, the morphology changes of the Al current collector cannot be found by these observations.

TEM-EELS measurements.— Transmission electron microscopy-electron energy loss spectroscopy (TEM-EELS) measurements of the positive electrode were conducted after 1000 cycles at 60°C, with the electrode in the fully discharged state. The sample for TEM-EELS measurements was prepared by Ar-ion milling from both sides of the electrode. No appreciable radiation damage associated with the high-energy electron exposure were observed during the measurements.

XAFS measurements.— Each positive electrode was investigated using X-ray absorption fine structure (XAFS) spectroscopy after setting potentials at 3.0, 3.65, 3.78, 4.0, and 4.2 V (vs Li^+/Li) with three electrode cells using the CC-CV protocol already mentioned.

The amount of deintercalated lithium, x in $Li_{1-x}Ni_{0.8}Co_{0.15}Al_{0.05}O_2$, was determined using inductively coupled plasma-atomic emission spectroscopy (ICP-AES). The Li and Ni concentrations were obtained using ICP-AES, and the Li composition was calculated from the Li/Ni molar ratio, assuming that the Ni composition is 0.8. The transmission XAFS measurements were performed on the beamline BL16B2 of SPring-8 (Hyogo, Japan). The beam size at the sample position was 1 × 5 mm. The energy calibration of the monochromator was performed using a 6 μm thick Ni foil. Ni *k*-edge X-ray absorption near-edge structure (XANES) spectra were analyzed using an REX2000 (Rigaku Corp.).

Results and Discussion

Capacity fade.— Changes in the discharge capacities of the cylindrical batteries with cycle number at 20–80°C, normalized by the weight of positive active materials, are shown in Fig. 1. With the increase in cycling temperature, the capacity fade with cycling was accelerated and was particularly conspicuous for the battery cycled at 80°C. The capacity fade of the batteries at 20°C and 0.1 C rate after 500 cycles are summarized in Table I, together with those of the corresponding positive electrodes measured using three electrode half-cells. In the case of cycling at 80°C, the capacity fade of the positive electrode is almost the same as that of the battery itself. This indicates that the capacity fade during cycling at 80°C is derived from degradation of the positive electrode. In the case of cycling at 20 and 60°C, the results in Table I suggest that some other factors such as lithium-ion loss by SEI formation on the anode[25] seem to be overlaid on the degradation of the positive electrode in the total capacity fade.

In the following subsections, we focus on the capacity fade of positive electrodes after cycling tests at 20–80°C, because the origin of the capacity fade in the $LiNiO_2$-based positive electrodes would have a significant influence on the cycle durability of lithium-ion batteries at elevated temperature.

Cyclic Voltammetry.— Figure 2 shows cyclic voltammetry curves of the positive electrodes before and after the cycling tests at 20–80°C. The cyclic voltammetry curves represent the electrochemical properties of the electrodes. Three peaks were observed in the cyclic voltammetry curve of the positive electrode before cycling on both oxidation and reduction regimes, which were caused by phase transitions that occur during deintercalation/intercalation of Li ions in the active material.[26,27] The peaks of the degraded positive electrodes could not be clearly observed as the cycling temperature increased. These results indicate that the positive electrodes suffer from not only capacity fade but also increase in impedance by

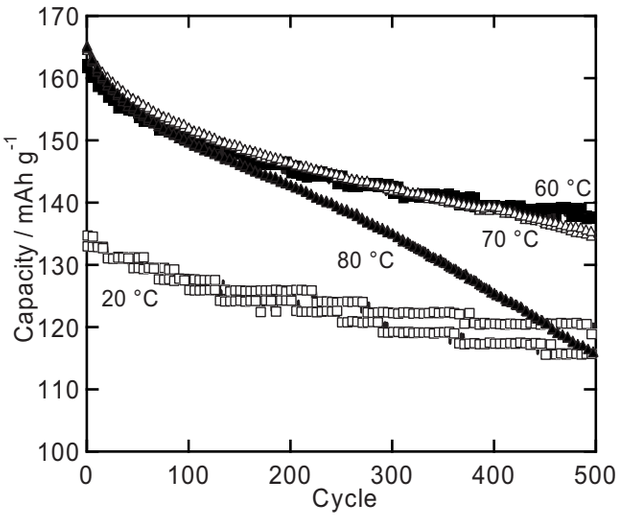

Figure 1. Change in capacity during cycling tests with a 2 C rate at 20, 60, 70, and 80°C.

Table I. Capacity fade of batteries and positive electrodes after 500 cycles.

Cycle temperature (°C)	Capacity fade of battery (mAh g^{-1})	Capacity fade of positive electrode (mAh g^{-1})
20	7.2	2.3
60	16.5	10.6
80	53.5	47.8

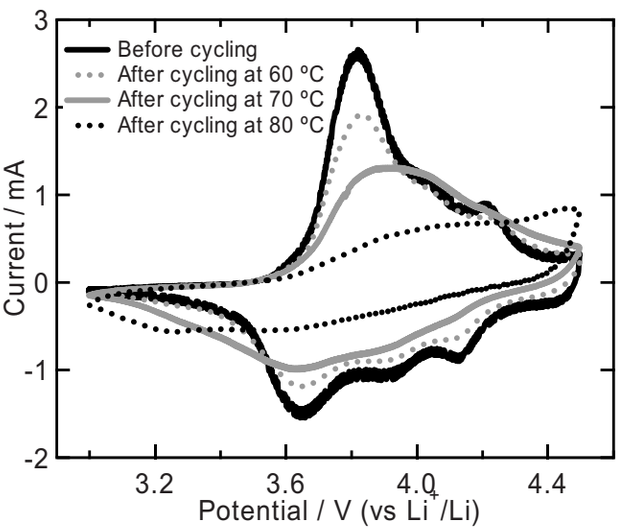

Figure 2. Cyclic voltammograms of the positive electrodes before and after cycling tests at 60, 70, and 80°C.

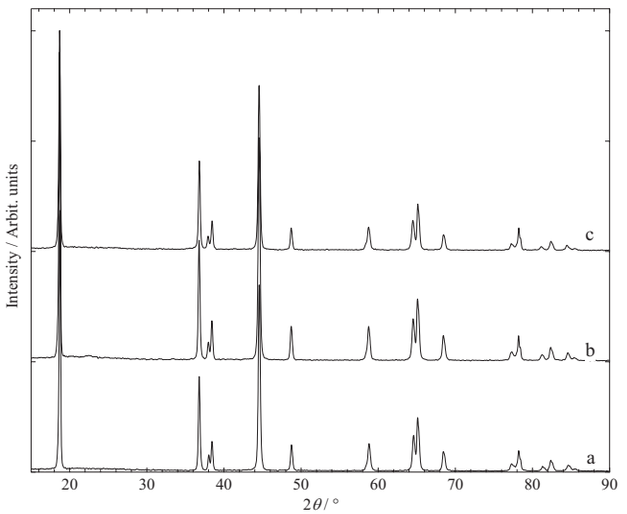

Figure 3. XRD patterns for the positive electrodes (a) before cycling test, (b) after cycling test at 60°C, and (c) after cycling test at 80°C.

cycling at elevated temperatures. And, deterioration of the positive electrodes was also confirmed by the cyclic voltammetry method.

XRD analysis.— Figure 3 shows XRD patterns of the positive electrodes before and after cycling at 60 and 80°C in the fully discharged state. The XRD analysis failed to detect any noticeable change, as in previous papers.[9]

EELS analysis.— Figure 4a shows a typical Ni-$L_{2,3}$ energy-loss near-edge structure (ELNES) spectrum from the active $Li_{1-x}Ni_{0.8}Co_{0.15}Al_{0.05}O_2$ material in the positive electrode after 1000 cycles at 60°C. The spectrum is consistent with that from Ni(III) in $LiNi_{0.8}Co_{0.15}Al_{0.05}O_2$,[28] which is reasonable because the active material in this sample remains in the fully discharged state. We often encountered other types of ELNES spectra, a typical example of which is shown in Fig. 4b. This spectral profile is similar to that of Ni(II) in NiO.[29] Ni(II) should not exist in ideal Ni-based active materials in the potential range between 3.0 and 4.2 V; therefore, this result suggests that Ni(II) was formed during the cycling tests. Because such a deteriorated phase is partly localized at some regions and partly dispersed as fine grains/domains, as will be shown in Part II of this series paper, various mixture spectra of the spectral profiles in Fig. 4a and b were often observed. It is not yet

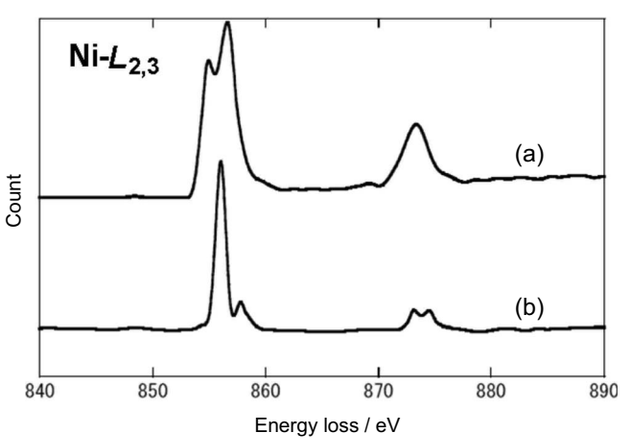

Figure 4. Ni-$L_{2,3}$ ELNES spectra taken from the sample after 1000 cycles at 60°C: (a) normal part and (b) anomalous part.

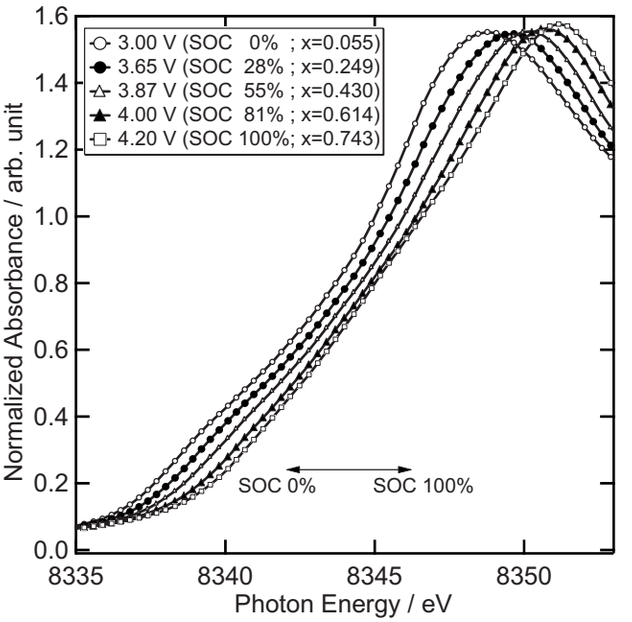

Figure 5. Ni K-edge XANES spectra for the as-prepared positive electrode in various SOC.

clear whether those mixture spectra are derived from continuous intermediate states or mixtures from small grains of both phases. These speculations seem to be consistent with the XRD results mentioned above. The amount of Ni(II) formed is estimated in the following section using XAFS measurements.

XAFS analyses.— A set of Ni K-edge XANES spectra of the fresh positive electrode in a variety of states of charge (SOC) is shown in Fig. 5. As expected, the edge onset is shifted to the higher-energy side with increasing x in $Li_{1-x}Ni_{0.8}Co_{0.15}Al_{0.05}O_2$, the fraction of Li deintercalation, because Ni(III) is oxidized to Ni(IV).[30] Figure 6 shows Ni K-edge XANES spectra of

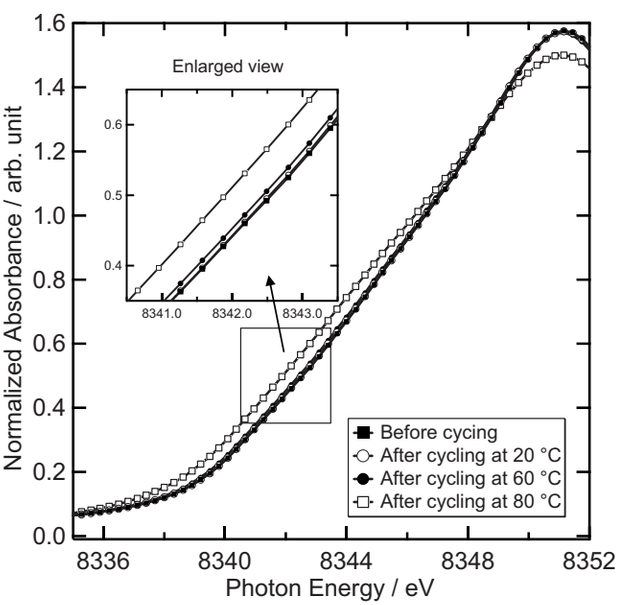

Figure 6. Ni K-edge XANES spectra of $Li_{1-x}Ni_{0.8}Co_{0.15}Al_{0.05}O_2$ at 4.2 V before and after 500 cycling tests at 20, 60, and 80°C.

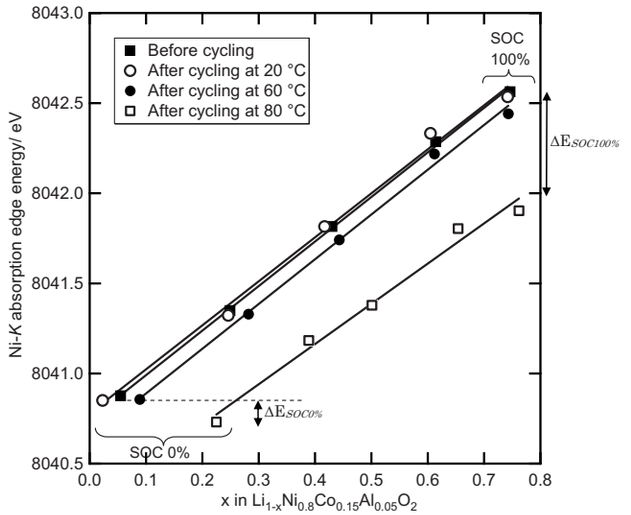

Figure 7. Comparison of the energies at the half-step heights of Ni K-edge XANES spectra as a function of x in $Li_{1-x}Ni_{0.8}Co_{0.15}Al_{0.05}O_2$ before and after the cycling tests.

$Li_{1-x}Ni_{0.8}Co_{0.15}Al_{0.05}O_2$ charged at 4.2 V before and after 500 cycles at 20, 60, and 80°C. After cycling at 60 and 80°C, the Ni K-edge spectra are clearly shifted to the lower energy side, which indicates that Ni is reduced to a lower valence. Therefore, a lesser fraction of Ni ions are able to change into Ni(IV), even at the 4.2 V charged state, after cycling at elevated temperatures. To evaluate the reduction of Ni ions more quantitatively, the relationship between the amount of Li deintercalation (x in $Li_{1-x}Ni_{0.8}Co_{0.15}Al_{0.05}O_2$) and the Ni valence was investigated before and after the cycling tests. The energy at half-step height (where normalized absorbance = 0.5) was used as a measure of Ni valence.

Figure 7 shows a comparison of the energies at the half-step heights of the Ni K-edge XANES spectra as a function of x in $Li_{1-x}Ni_{0.8}Co_{0.15}Al_{0.05}O_2$ before and after the cycling tests. The smallest and largest x for each sample correspond to SOC 0% (3.0 V vs Li^+/Li) and SOC 100% (4.2 V vs Li^+/Li), respectively. The data points obey a linear relationship, with slopes that are almost identical to one another, indicating that the amount of oxidized Ni ions is proportional to the amount of Li deintercalation, even after cycling at elevated temperatures. However, as observed for the data of SOC 100%, the Ni valence is more reduced with the increase in cycling temperature than that of the fresh sample at the same value of x. These changes indicate that a certain fraction of Ni(IV) ions is reduced to lower valency, Ni(III) or Ni(II), without Li intercalation during cycling at elevated temperatures. These anomalous Ni ions can no longer change their valence by further Li intercalation/deintercalation reactions in the potential range between 3.0 and 4.2 V, and they then act as "inactive Ni ions." The formation of such inactive Ni ions is not attributable to the structural degradation of the electrode composites but to the microscopic degradation of the active material itself. This is consistent with the EELS results. Furthermore, if the capacity fade results merely from particle isolation from the conducting additive connection, the relationship between Li composition and Ni valence must remain unchanged.

Previous researchers have reported that formation of NiO-like surface layers in active materials is important in electrode impedance rise.[17,18] The formation of NiO-like structure would be partially relevant to the capacity fade by the formation of inactive Ni ions, and particle isolation by NiO-like surface layers would not mainly contribute to the capacity fade in this study by the reason mentioned above.

In order to clarify the relationship between the amount of inactive Ni ions and the capacity fade, the following quantitative analysis was conducted. For each sample, the slope of the linear relationship of the Ni K-edge energy vs x in $Li_{1-x}Ni_{0.8}Co_{0.15}Al_{0.05}O_2$ was quantitatively obtained by least-squares fitting. The fitted lines are shown in Fig. 7, and the slopes and intercepts are tabulated in Table II. Mansour et al. investigated the relationship between the valence of Ni ions and the Ni K-edge energy (as measured at half-step height) for various Ni compounds and reported that the chemical shift accompanied by oxidation from Ni(III) to Ni(IV) is 2.46 and 1.24 eV for the change from Ni(II) to Ni(III), respectively.[31] The present values of 2.23–2.48 eV are in good agreement with the chemical shift from Ni(III) to Ni(IV), and therefore quantitative analysis can be estimated based on the data as follows.

Table II. Slopes and intercepts of the least-squares fitted lines shown in Fig. 7.

Sample condition	Slope	Intercept
Before cycling	2.47 ± 0.04	8340.74 ± 0.02
Cycling at 20°C	2.44 ± 0.11	8340.78 ± 0.06
Cycling at 60°C	2.48 ± 0.08	8340.64 ± 0.04
Cycling at 80°C	2.23 ± 0.16	8340.27 ± 0.09

The fraction of "inactive Ni ions," Ni(III) or Ni(II), can be estimated from the energy shift between the states before and after cycling at SOC 100%, because almost all the active Ni ions in the positive electrode should be Ni(IV) at SOC 100% (4.2 V vs Li^+/Li). First, the ratio of the inactive Ni(II) to the total inactive Ni ions must be determined, because Ni(II) has to be counted twice for estimation of the average Ni valence change, and the data points of SOC 0% in Fig. 7 can be used. At SOC 0% (3.0 V vs Li^+/Li), all the Ni ions available (active) in the positive electrode should be Ni(III), whereas the Ni K-edge energies after cycling at elevated temperatures are slightly smaller than that before the cycling tests, despite the nominal increase in x, which is attributable to the formation of Ni(II). The procedure for estimating the amount of inactive Ni ions after cycling utilizes these energy shifts and is summarized as follows.

Estimation of the fraction of inactive Ni(II) after cycling from the SOC 0% data.— Because the Ni ions at SOC 0% before cycling should be Ni(III), the redshift of Ni K-edge at SOC 0% after cycling is attributable to formation of Ni(II). The energy shift is denoted as $\Delta E_{SOC0\%}$, as indicated in Fig. 7. Assuming that the Ni valence is linearly correlated with the Ni K-edge energy, we can estimate the amount of Ni(II) from $\Delta E_{SOC0\%}$ by the following equation using the reference chemical shift from Ni(III) to Ni(II), 1.24 eV[31]

$$Q_{Ni(II)} = \Delta E_{SOC0\%}/1.24 \quad [1]$$

where $Q_{Ni(II)}$ is the fraction of inactive Ni(II) in the total Ni ions.

Estimation of energy shift due to the formation of inactive Ni(III) at SOC 100%.— Almost all the active Ni ions before cycling should be Ni(IV) at SOC 100%. The redshift of Ni K-edge energy at SOC 100% after cycling is thus attributable to transformation of the active Ni(IV) to inactive Ni(II) or Ni(III). Because the fraction of inactive Ni(II), $Q_{Ni(II)}$, was already estimated from Eq. 1, the net redshift associated with the formation of inactive Ni(III) is estimated from the following equation using the reference chemical shift from Ni(II) to Ni(IV), 3.70 eV[31]

$$\Delta E_{Ni(III)} = \Delta E_{SOC100\%} - 3.70 \times Q_{Ni(II)} \quad [2]$$

where $\Delta E_{SOC100\%}$ and $\Delta E_{Ni(III)}$ are, respectively, the energy shift between the states before and after cycling at SOC 100% and that due to the formation of inactive Ni(III) at SOC 100%.

Estimation of the fraction of inactive Ni(III) after cycling from $\Delta E_{Ni(III)}$.— The fraction of inactive Ni(III) can be estimated in the same manner as in the first estimation from $\Delta E_{Ni(III)}$ and the reference chemical shift associated with the transformation from Ni(III) to Ni(IV), 2.46 eV[31]

Table III. $\Delta E_{SOC0\%}$, $\Delta E_{SOC100\%}$, $Q_{Ni(II)}$, $Q_{Ni(III)}$, and Q_{total} for samples after cycling tests at 60 and 80°C.

Cycling temperature (°C)	$\Delta E_{SOC0\%}$ (eV)	$\Delta E_{SOC100\%}$ (eV)	$Q_{Ni(II)}$ (%)	$Q_{Ni(III)}$ (%)	Q_{total} (%)
60	0.020	0.123	1.61	2.57	4.18
80	0.146	0.661	11.8	9.16	20.9

$$Q_{Ni(III)} = \Delta E_{Ni(III)}/2.46 \quad [3]$$

where $Q_{Ni(III)}$ is the fraction of inactive Ni(III) in the total Ni ions. *Estimation of the total amount of inactive Ni ions.*— Finally, the total amount of inactive Ni ions, Q_{total}, is estimated from $Q_{Ni(II)}$ and $Q_{Ni(III)}$ calculated in the first and third estimations

$$Q_{total} = Q_{Ni(II)} + Q_{Ni(III)} \quad [4]$$

where Q_{total} is the fraction of total inactive Ni in the total Ni ions.

The estimated values of $\Delta E_{SOC0\%}$, $\Delta E_{SOC100\%}$, $Q_{Ni(II)}$, $Q_{Ni(III)}$, and Q_{total} for the samples after the cycling tests are summarized in Table III. The amounts of inactive Ni(II) and Ni(III) in the positive electrode were, respectively, 11.8 and 9.2% after cycling at 80°C and 1.61 and 2.57% after cycling at 60°C. The fraction of Ni(II) in the total inactive Ni ions was significantly increased with the increase in cycling temperature.

The capacity fade caused by the formation of inactive Ni ions can be calculated from the estimated inactive Ni composition and the theoretical capacity of $Li_{1-x}Ni_{0.8}Co_{0.15}Al_{0.05}O_2$ ($x = 0$–1), 278.95 mAh g^{-1}. The fraction of inactive Ni ions (Q_{total}) in the total Ni ions, the corresponding inactive Ni compositions, and the estimated capacity fade are summarized in Table IV, along with the measured capacity fade of the positive electrode already shown in Table I. The estimated values correspond well with the measured capacity fade. The quantitative analysis strongly indicates that the formation of inactive Ni ions, due to the reduction of Ni ions and without Li intercalation, is the most dominant factor in the capacity fade of the positive electrode. Loss of oxygen in the active material during cycling at elevated temperatures would be associated with the formation of reduced Ni ions without Li intercalation, and this will be discussed in the second part of this series.

In addition, the subsequent paper in this series will intensively examine the structure and spatial distribution of the degraded phase in the active material by means of TEM and spectroscopic imaging.

Conclusion

Several diagnostic techniques were employed to investigate the mechanism for capacity fade in lithium-ion batteries with $LiNiO_2$-based positive electrodes after cycling at elevated temperatures. Electrochemical analyses showed that the capacity fade of the batteries was mainly caused by degradation of the positive electrode, particularly after cycling at 80°C. EELS and XAFS analyses revealed the formation of Ni ions with lower valence than expected in the $LiNiO_2$-based active material, and those reduced Ni ions are thought to be inactive for Li intercalation/deintercalation reactions. Quantitative analyses using XAFS revealed that the inactive Ni(II) and Ni(III) in the positive electrode after cycling at 80°C amounted to 11.8 and 9.2%, respectively. The estimated fractions of inactive Ni ions provide a suitable quantitative explanation for the measured capacity fade of the positive electrodes.

Table IV. Fraction of total inactive Ni ions, inactive Ni compositions, and estimated and measured capacity fades for samples after cycling tests at 60 and 80°C.

Cycling temperature (°C)	Total inactive Ni (Q_{total}) (%)	Inactive Ni composition	Estimated capacity fade (mAh g^{-1})	Measured capacity fade (mAh g^{-1})
60	4.18	0.0334	9.33	10.6
80	20.9	0.167	46.7	47.8

Acknowledgments

The authors thank O. Hiruta, T. Kobayashi, S. Kawauchi, H. Kondo, M. Hasegawa, and Y. Makimura for valuable discussion and technical support, K. Horibuchi for TEM-EELS measurements, and I. Tajima, H. Nozaki, and S. Yamaguchi for XAFS measurements. We also thank H. Tanida for developing the software for the XAFS measurements.

Toyota Central Research and Development Laboratories, Inc. assisted in meeting the publication costs of this article.

References

1. J. R. Dahn, U. von Sacken, M. W. Juzkow, and H. Al-Janaby, *J. Electrochem. Soc.*, **138**, 2207 (1991).
2. C. Delmas, I. Saadoune, and A. Rougier, *J. Power Sources*, **44**, 595 (1993).
3. T. Ohzuku, A. Ueda, and M. Kouguchi, *J. Electrochem. Soc.*, **142**, 4033 (1995).
4. M. Brousselya, P. Blanchard, P. Biensan, J. P. Planchata, K. Nechevc, and R. J. Staniewiczc, *J. Power Sources*, **119–121**, 859 (2003).
5. S. Madhavi, G. V. Subba Rao, B. V. R. Chowdari, and S. F. Y. Li, *J. Power Sources*, **93**, 156 (2001).
6. M. Guilmard, C. Pouillerie, L. Croguennec, and C. Delmas, *Solid State Ionics*, **160**, 39 (2003).
7. C. H. Chen, J. Liu, M. E. Stoll, G. Henriksen, D. R. Vissers, and K. Amine, *J. Power Sources*, **128**, 278 (2004).
8. R. B. Wrighta, J. P. Christophersena, C. G. Motlocha, J. R. Belta, C. D. Hoa, V. S. Battagliab, J. A. Barnesc, T. Q. Duongc, and R. A. Sutula, *J. Power Sources*, **119–121**, 865 (2003).
9. J. Shim, R. Kostecki, T. Richardson, X. Song, and K. A. Striebel, *J. Power Sources*, **112**, 222 (2002).
10. Y. Itou and Y. Ukyo, *J. Power Sources*, **146**, 39 (2005).
11. J. P. Christophersen, C. D. Ho, C. G. Motloch, D. Howell, and H. L. Hess, *J. Electrochem. Soc.*, **153**, A1406 (2006).
12. M. Dubarry, V. Svoboda, R. Hwu, and B. Y. Liaw, *J. Power Sources*, **165**, 566 (2007).
13. H. Kondo, Y. Takeuchi, T. Sasaki, S. Kawauchi, Y. Itou, O. Hiruta, C. Okuda, M. Yonemura, T. Kamiyama, and Y. Ukyo, *J. Power Sources*, **174**, 1131 (2007).
14. K. Amine, C. H. Chen, J. Liu, M. Hammond, A. Jansen, D. Dees, I. Bloom, D. Vissers, and G. Henriksen, *J. Power Sources*, **97–98**, 684 (2001).
15. C. H. Chen, J. Liu, and K. Amine, *J. Power Sources*, **96**, 321 (2001).
16. C. H. Chen, J. Liu, and K. Amine, *Electrochem. Commun.*, **3**, 44 (2001).
17. D. P. Abraham, R. D. Twesten, M. Balasubramanian, I. Petrov, J. McBreen, and K. Anine, *Electrochem. Commun.*, **4**, 620 (2002).
18. D. P. Abraham, R. D. Twesten, M. Balasubramanian, J. Kropf, D. Fischer, J. McBreen, I. Petrov, and K. Anine, *J. Electrochem. Soc.*, **150**, A1450 (2003).
19. A. M. Andersson, D. P. Abraham, R. Haasch, S. MacLaren, J. Liu, and K. Amine, *J. Electrochem. Soc.*, **149**, A1358 (2002).
20. R. Kostecki and F. McLarnon, *Electrochem. Solid-State Lett.*, **5**, A164 (2002).
21. T. C. Hyams, J. Go, and T. M. Devinea, *J. Electrochem. Soc.*, **154**, C390 (2007).
22. R. Kostecki, J. Lei, F. McLarnon, J. Shim, and K. Striebel, *J. Electrochem. Soc.*, **153**, A669 (2006).
23. T. Nonaka, C. Okuda, Y. Seno, Y. Kondo, K. Koumoto, and Y. Ukyo, *J. Electrochem. Soc.*, **154**, A353 (2007).
24. H. Kobayashi, M. Shikano, S. Koike, H. Sakaebe, and K. Tatsumi, *J. Power Sources*, **174**, 380 (2007).
25. P. Ramadass, B. Haran, R. White, and B. N. Popov, *J. Power Sources*, **112**, 606 (2002).
26. T. Ohzuku, A. Ueda, and M. Nagayama, *J. Electrochem. Soc.*, **140**, 1862 (1993).
27. K. Dokko, M. Nishizawa, S. Horikoshi, T. Itoh, M. Mohamedi, and I. Uchida, *Electrochem. Solid-State Lett.*, **3**, 125 (2000).
28. J. Graetz, C. C. Ahn, R. Yazami, and B. Fultz, *J. Phys. Chem. B*, **107**, 2887 (2003).
29. C. Mitterbauera, G. Kothleitnera, W. Groggera, H. Zandbergenb, B. Freitagc, P. Tiemeijerc, and F. Hofera, *Ultramicroscopy*, **96**, 469 (2003).
30. T. Nonaka, C. Okuda, Y. Seno, H. Nakano, K. Koumoto, and Y. Ukyo, *J. Power Sources*, **162**, 1329 (2006).
31. A. N. Mansour, J. McBreen, and C. A. Melendresc, *J. Electrochem. Soc.*, **146**, 2799 (1999).